COMPARISON AND VALIDATION OF THE FRANCE/USA FINITE STATE ROTOR DYNAMIC INFLOW MODELS

Pierre-Marie Basset
ONERA, DCSD-PSEV
System Control and Flight Dynamics department
Salon-de-Provence, FRANCE
basset@onera.fr

Robert A. Ormiston
Aeroflightdynamics Directorate (AFDD- ARMDEC)
US Army Research, Development, and Engineering Command
Ames Research Center, Moffett Field, California, USA
robert.ormiston@us.army.mil

Notation

b	number of blades,
c	blade chord, (m)
C_m, C_d, C_l	pitch, drag and lift coefficients,
FSDI	general abbreviation for Finite State Dynamic Inflow
FiSuW	Finite State Unsteady Wake model (=FSDI in HOST)
HOST	Helicopter Overall Simulation Tool (Eurocopter-ONERA rotorcraft simulation code)
IS	Inflow States
μ	advance ratio : $V_h/(\Omega.R)$,
Ω	rotor rotational speed, (rad/s)
r	radial position of a point on the rotor, (m)
R	rotor radius, (m)
$\bar{r}$	non-dimensional radial position $\bar{r} = r/R$
RCAS	Rotorcraft Comprehensive Analysis System, AFDD simulation code
ρ	air density, (kg/m^3)
$\bar{t}$	non-dimensional time $\bar{t} = \Omega.t$
TPP	rotor blade Tip Path Plane
V_{iz} or w_i	induced velocity normal to the rotor, (m/s) or (ft/s)

Abstract

In the framework of the MoA between France and USA on "Helicopter Aeromechanics", a task is dedicated to rotorcraft flight dynamics. The overall objective of the collaborative effort in the flight mechanics area is to improve the prediction capability of the simulation codes. That is why a special attention is devoted to the Finite State Dynamic Inflow modelling approach which is particularly well adapted for rotorcraft flight dynamics. The paper will present comparisons of our finite state dynamic inflow models: between partners, with respect to NASA Langley wind-tunnel data, with respect to other modeling approaches (e.g. vortex wake models).

Presented at the 36th European Rotorcraft Forum, Paris, France, September 7-9, 2010.

Introduction

In the framework of the MoA between France and USA on "Helicopter Aeromechanics", a task is dedicated to the rotorcraft flight dynamics. The overall objective of the collaborative effort in the flight mechanics area is to improve the prediction capability of the simulation codes dedicated to rotorcraft flight dynamics. Within this task, a topic is addressed during a period about three years. This paper presents a synthesis on the last topic of collaboration between ONERA and AFDD which was devoted to the Finite State Rotor Dynamic Inflow modelling.

This rotor inflow modelling approach is particularly well adapted for studies of rotorcraft flight dynamics, as well as for rotor dynamics, etc. Indeed it offers a description of the rotor induced velocity field in a finite state formulation which is well suited for:

- choosing the resolution, or level of detail of the rotor inflow distribution (high number of inflow states for applications requiring high fidelity models, low number of inflow states for applications putting the emphasis on the quickness of the computation as for real-time simulations);
- linearization and stability studies because a finite number of inflow states are clearly defined and the model provides their dynamics in closed form.

The rotor dynamic inflow theory applied here is based on the work of the Professor Peters (e.g. [1][2][3][4]) and his students. This paper acknowledges his singular contribution in developing a model for such a complex phenomenon (rotor inflow dynamics) in a clear mathematical form well founded on potential flow physics. Compared to other modelling approaches like the various vortex wake methods, the approach is more analytical than numerical in the sense that a constant effort was pursued to provide closed form expressions. Hereafter the modelling basis is briefly reviewed, presenting the common theoretical foundations and the differences in the implementations respectively in HOST and RCAS.

After concisely describing the wind-tunnel measurements, the paper will present comparisons of our finite state dynamic inflow calculations: between partners, with respect to NASA Langley wind-tunnel data,

with respect to other modeling approaches (e.g. vortex wake models). Finally the rotor inflow calculations with RCAS and HOST will be compared on a simplified academic case in order to better assess their agreement. A special contribution of this paper is to draw the attention of the reader on the different kinds of rotor inflow measurements and calculations.

Description of the HOST and RCAS Models

This section of the paper will briefly describe the Finite State Dynamic Inflow theory and its implementation in the HOST and RCAS rotorcraft computer codes.

Common foundations

The formulation of the Finite State Dynamic Inflow theory that is used herein for both HOST and RCAS is based on the model presented by He ([1]-[2]-[3]). Subsequently an even more general formulation was developed by Peters and his students using a Galerkin approach to embrace not only the rotor inflow dynamics on the rotor disk, but also the entire flowfield above and below the rotor disk (e.g. [4]). The theory presently employed in HOST and RCAS and for this paper is the Peters-He theory.

The basic idea is to find a representation of rotor inflow dynamics in which the states are clearly identified, not too numerous, and for which physically-based governing differential equations can be obtained.

Instead of searching a state space representation for the wake itself, the modelling effort was focused on effect of the wake, more precisely on the rotor induced flowfield. The most well-known contributors to the first harmonic rotor downwash modelling include Froude (mean downwash v_{i0}, [6]), Glauert (plus longitudinal gradient v_{i1c} due to the skewed wake in forward flight [6]), Meijer-Drees (plus lateral gradient v_{i1s} linked to the non-symmetry between the advancing and retreating sides in forward flight [7]). Later researchers proposed other analytical laws for computing the inflow gradients (e.g. Coleman [8], Blake and White [9]). These simple analytical models assume implicitly that the inflow reacts quasi-instantaneously to the variations of the airspeed conditions and of the rotor airloads.

Peters took a significant step forward by developing a dynamic inflow theory. Today, the Pitt and Peters model ([10] to [12]) is probably the most widely used rotor inflow model in the rotorcraft flight dynamics simulation world. Nevertheless, this model is limited to the first harmonic and a linear radial inflow distribution along the blade span. Peters and He proposed ([1] to [3]) a more comprehensive theory for an arbitrary number of harmonics and non-linear radial inflow distributions.

Both models ([1] and [10]) are based on an acceleration potential approach. The assumptions under which the airflow can be described by an acceleration potential are less demanding than the ones required for a velocity potential. Indeed, the existence of a velocity potential would require that the airflow be irrotational, which is not suitable for describing the airflow through a rotor.

The assumptions for the existence of an acceleration potential are the ones required for having:

$$\overrightarrow{rot}\left(\frac{d\vec{V}}{dt}\right)=\vec{0}\Leftrightarrow\overrightarrow{rot}\left(\frac{d\vec{V}}{dt}\right)=\frac{\overrightarrow{grad}\rho\wedge\overrightarrow{grad}P}{\rho^2}+\overrightarrow{rot}.\vec{F}=\vec{0}$$

Thus for the acceleration derives from a potential, the following conditions must be fulfilled:

- the mass force $\vec{F}$ must derived from a potential, as is always the case for the gravity force:

$$\overrightarrow{rot}\vec{F}=\overrightarrow{rot}\left(\overrightarrow{grad}(mg)\right)=\vec{0}$$

- the airflow must be either incompressible:

$$\rho=const.\Rightarrow\overrightarrow{grad}\rho=\vec{0}\Rightarrow\overrightarrow{grad}\rho\wedge\overrightarrow{grad}P=\vec{0}$$

or at least barotropic. Indeed, such a fluid flow is said barotropic if a function, f(P, ρ), relating the local pressure and density, exists throughout the flowfield and is constant (i.e., independent of time and space), which leads to:

$$\overrightarrow{grad}\rho\wedge\overrightarrow{grad}P=\vec{0}$$

(That is, for example, the case of homentropic flows for which the entropy is such a function: S(P, ρ)=constant).

The helicopter normally operates within an incompressible perfect airflow. That is especially the case at low speeds which is the specific domain of helicopters and where the influence of the rotor wake is the most important. At high speeds the transonic flow near the tip of the advancing blade may violate the incompressible condition, but that occurs at "the edge of the flight domain".

From the mathematical point of view, assuming the existence of an acceleration potential reduces the number of unknowns, because the three-dimensional vector representing the airflow acceleration is replaced by a scalar function representing the perturbation of the acceleration potential. The perturbations due to the variations of the airspeed conditions and/or the rotor airloads are captured by the acceleration potential (ϕ) scalar function which relates to the associated rotor inflow dynamics. This connection is done through the fundamental fluid mechanics equations (conservation of mass and momentum), which provide the differential equations governing the dynamic response of the inflow to the airload and airspeed variations.

The presentation proposed here, shows that this finite state dynamic inflow theory is inspired by the "Proper Orthogonal Decomposition" (POD) method (e.g. [13]). The POD techniques allow transforming a partial derivative equation into an ordinary differential equation. In order to be decomposed into mono-dimensional variables, the physical multi-dimensional variable of

interest (for example the airflow acceleration potential or the induced velocity which are both time and space dependent $\phi(t, x, y, z)$), must be projected on an orthogonal basis. One difficulty is to determine suitable mode shape functions to represent the vectors of this orthogonal basis.

For the choice of an appropriate basis, both models ([1] and [10]) followed the approach of Kinner [14], who first demonstrated that Legendre functions in ellipsoidal coordinates are well-suited to rotor aerodynamic analyses. Indeed, these Legendre functions allow modelling a discontinuity through a circular disk, while still satisfying Laplace's equation. Therefore these orthogonal functions are ideal candidates to represent the pressure field associated with a rotor disk, since, as is well-known, the flow through a lifting rotor experiences a discontinuity of pressure. For the azimuthal variations (of pressure and induced flow), the classical Fourier decomposition is applied.

Laplace's partial differential equation expressed in the ellipsoidal coordinate system, can be divided into three ordinary differential equations (ODE). The general forms of the solutions of these ODEs are based on trigonometric functions (cos(hψ and sin(hψ)) and Legendre's associated functions.

Therefore, each component of the induced velocity vector at a point on the rotor may be expressed through a double expansion. For example the normal component to the rotor disk is written as:

$$w_i(\bar{r},\psi,\bar{t}) = \sum_{h=0}^{\infty} \sum_{\substack{f=h+1,\\ h+3,....}}^{\infty} \phi_f^h(\bar{r}) \times \left[{w_{ic}}_f^h(\bar{t}).\cos(h\psi) + {w_{is}}_f^h(\bar{t}).\sin(h\psi) \right] \quad (1)$$

- where Fourier's series represents the azimuthal variations (h is the number of harmonics) and,
- Legendre's polynomials represent the radial distributions (f is the radial mode shape number associated with the harmonic h).

And where $(\bar{r}, \bar{t})$ are the non-dimensional radius and time variables: $(\bar{r} = r/R, \bar{t} = \Omega.t)$.

The radial shape functions $\left(\phi_f^h\right)$ correspond to the normalized Legendre polynomials of the first kind. The standard normalization is done for $(\bar{r} \in [-1,1])$. In order to have an orthonormal basis adapted to describe the radial inflow distribution along the blade span [0,1], these radial functions are divided by the ellipsoidal coordinate $\left(\nu = \sqrt{1-\bar{r}^2}, \text{ on the rotor}\right)$:

$$\phi_f^h = \frac{\bar{P}_f^h(\nu)}{\nu}$$

According to the POD interpretation, the time dependent inflow states: $\left({w_{ic}}_f^h\right)$ for the cosine terms and $\left({w_{is}}_f^h\right)$ for the sine terms, are the eigen-modes of the induced flow field on the rotor. Their dynamics are governed by the first order differential equations coming from the fundamental mass and momentum conservation equations:

$$\overbrace{[M].\left\{\begin{matrix}\vdots\\ {}^{*}{w_{ic}}_f^h\\ \vdots\end{matrix}\right\}}^{Unsteadiness} + \overbrace{\left[\tilde{L}_c\right]^{-1}.[V].\left\{\begin{matrix}\vdots\\ {w_{ic}}_f^h\\ \vdots\end{matrix}\right\}}^{Convection\ part} = \overbrace{\frac{1}{2}\left\{\begin{matrix}\vdots\\ {\tau_c}_f^h\\ \vdots\end{matrix}\right\}}^{Excitation}$$

$$[M].\left\{\begin{matrix}\vdots\\ {}^{*}{w_{is}}_f^h\\ \vdots\end{matrix}\right\} + \left[\tilde{L}_s\right]^{-1}.[V].\left\{\begin{matrix}\vdots\\ {w_{is}}_f^h\\ \vdots\end{matrix}\right\} = \frac{1}{2}\left\{\begin{matrix}\vdots\\ {\tau_s}_f^h\\ \vdots\end{matrix}\right\}$$

The details of the derivation of these FSDI equations were given in [3] including the principal terms:

- the apparent-mass matrix [M] for the dynamics part of the model,
- the gain matrices [L] for the convection part of the model,
- the vector of the generalised pressure forces [τ] representing the rotor airload excitations.

The diagonal mass-flow parameters matrix [V] is calculated as follows:

$$V_1^0 = V_T = \sqrt{\mu^2 + \lambda^2}$$

$$V_f^h = V = \frac{\mu^2 + \lambda.(\lambda + \lambda_m)}{\sqrt{\mu^2 + \lambda^2}}, \quad \text{for } (h,f) \neq (0,1)$$

where (μ) is the advance ratio and (λ) is the total vertical flow velocity through the rotor:

$$\lambda = \lambda_m + V_\infty \times \sin\alpha$$

and (λ_m) is the mean inflow parameter from which comes the non-linearity of the model since it depends on the inflow states (see the paragraph below "Implementations of FSDI in HOST and RCAS").

To sum up, the inputs are the airspeed conditions (the wake skew angle for example which enters into the gain matrices calculation) and the rotor lift distribution from which are determined the generalised forces as excitation terms on the right hand side of the dynamic inflow equations. The analysis and decomposition of the rotor lift distribution in Fourier and Legendre's series are performed at the same order as the description of the induced velocity distribution on the rotor disk (in terms of harmonics and order of the radial mode shapes). The

outputs of the model are the inflow states dynamics given by the closed form differential equations of the first order in time (eq. 1).

Before leaving this section the Finite State Dynamic Inflow (FSDI) induced velocity will be briefly discussed. Several forms of the induced velocity will be addressed in this paper and it is important to clearly understand the differences and the terms used to describe them. The solution in Eq. (1) gives the induced velocity as a function of the location on the rotor disk, non-dimensional radius r/R and azimuth, ψ and also as a function of non-dimensional time, $\left(\bar{t} = \Omega.t\right)$. This means that the induced velocity is defined in a non-rotating (disk) reference frame and that it varies as a function of time at any point on the disk. The variation with time may be periodic or non-periodic, depending on the operation of the rotor. In a trimmed flight condition, the induced velocity will be periodic. In a maneuvering or transient condition, the induced velocity will be non-periodic. In any trimmed or periodic condition, the induced velocity at a point on the rotor disk will have an average value. We will refer to the time-varying and the average induced velocity at a point on the rotor disk as the ***time-varying*** and ***time-averaged*** induced velocities. For a non-periodic condition a time-averaged velocity will not exist. These induced velocities will hereafter be referred to as disk, or disk-referenced induced velocities. In terms of the FSDI theory of Eq (1), the time variation of induced velocity at a given point on the rotor disk (specified, constant ψ) will only be dependent on the time variation of the DI states (cosine and sine terms w_{ic}/w_{is}).

So far the motion or azimuthal position of the individual rotor blades has not been mentioned. For the disk induced velocities, the instantaneous, time varying velocity at a given point on the rotor disk will fluctuate with each blade passage. Typically, up-down velocity spikes will be produced by the blade bound vortex. Similar perturbations will occur for passage of trailing tip vortices convecting over the given point. (Note that the induction effects of the FSDI theory will only approximate the viscous nonlinear fluid effects that produce tightly rolled-up tip vortices in real flow fields). Note that the velocity perturbations associated with blade passage will not, of course, be present in the time-averaged induced velocities. Both the disk-referenced time varying and time-averaged induced velocities are relevant for experimental measurement of rotor flow fields such as the laser-velocimetry measurements that will be used later in this paper.

The other form of rotor induced velocity of interest here is the blade-referenced (or, on-blade) velocity, that is, the induced velocity at points on the rotor disk that coincide with the azimuthal location of the blade. It is a function of time in forward flight and may be periodic or non-periodic depending on the rotor operating condition. The on-blade induced velocity is important for the blade angle of attack and is calculated for all lifting-line-based rotor airloads analyses. Since the dimensionless time and the blade azimuth location are the same variable $\left(\bar{t} = \Omega.t = \psi_b\right)$, it is common to think of blade azimuth as the time variable in the case of blade-referenced induced velocity. For application of FSDI theory, time $\left(\bar{t}\right)$ must be distinguished from rotor disk azimuth (ψ) in Eq. (1). For a trimmed periodic operating condition, the blade induced velocity of Eq. (1) includes contributions from both the periodic time varying DI states and the periodic cosine/sine azimuth terms.

These different forms of induced velocity will be used in the next sections and later in the paper.

Implementations of FSDI in HOST and RCAS

A synthesis is presented regarding a careful comparison of the implementations of this modelling approach respectively in H.O.S.T. ("Helicopter Overall Simulation Tool", the rotorcraft simulation code created by Eurocopter and developed for years with contributions of ONERA, e.g. [15] to [20]) and in RCAS ("Rotorcraft Comprehensive Analysis System" the U.S. Army AFDD code, e.g. [21]). This discussion will focus on a clear identification of the differences in implementation of the FSDI theory in the two codes.

In summary three kinds of differences between our FSDI models have been identified during this collaboration:

1) Coordinate frame
   - FiSuW in HOST is implemented in the blade coordinate system,
   - FSDI in RCAS is implemented in the rotor TPP coordinate system.

The rationale for the RCAS implementation is that the FSDI theory is based on the potential flow solution for a circular wing supporting a pressure jump (normal force) across the disk and the associated normal (induced) velocity arising on the disk. Therefore, the rotor blade airloads are resolved into the rotor tip-path-plane (TPP) for determining the excitation forces that are input to FSDI theory. The differences between the HOST and RCAS coordinate frames are of course due the blade angles (controls and kinematics), i.e. pitch, flap and lead-lag angles. Therefore the final comparisons (for the simplified academic case addressed in a later section) have been done with: no twist, no flap, no lead-lag, and zero pitch angles.

2) Differences in the formulation

The mean inflow parameter $\left(\lambda_m\right)$ was initially calculated with different expressions leading to:

=> differences on the wake skew angle
=> differences on the mass flow parameters
=> therefore differences on the « gain matrices » and thus on the non-linearity of the model.

Indeed, (λ_m) depends on the axi-symmetrical inflow states (harmonic number 0):

- in RCAS - only on the first state, $\left(w_{ic1}^{0}\right)$, the model is therefore non-linear with respect to the first inflow state;
- in HOST – in the initial implementation the same simple expression was used, but then a more complete expression was introduced in order to take into account the effect of the other inflow states in an iterative computation in FiSuW (based on an expression provided in [2], eq. (2.89)).

The results for the comparison on the simplified academic case have been obtained by using the same simple expression in HOST for that term (λ_m) i.e. the momentum-theory value of the mean inflow for a trimmed rotor:

$$\lambda_m = \frac{C_T}{2V_T} \cong \sqrt{3} \times w_{ic1}^{\ 0}$$

3) Differences in the trim process

In both HOST and RCAS, the trim process for a steady state operating condition will encompass a periodic solution. A *periodic solution* refers to a rotorcraft analysis where the control variables (e.g., pilot controls or rotor controls such as cyclic and collective pitch) are fixed for a given steady-state flight or wind tunnel operating condition and a solution for the vehicle dynamic states is obtained by solving the nonlinear equations of motion. In steady-state forward flight, this solution is periodic. In forward flight, the steady-state *trim solution* encompasses the periodic solution but, in addition, satisfies *trim constraints* such that the control variables satisfy net rotor or vehicle forces corresponding to the vehicle or rotor operating condition. An iterative Newton-Raphson algorithm is used to iteratively adjust the control variables to satisfy the trim constraints.

In HOST, the *classic trim* computation is a "*harmonic trim*" in the sense that it applies a harmonic balance method. As explain in [19], the trim calculation method is based on a harmonic representation of the rotorcraft states. This representation is fully managed by HOST and the physical models never have to do harmonic-to-temporal transformations or harmonic analysis. All the models work in the time domain whether HOST is proceeding to a trim calculation or a time simulation. Therefore « averaged inflow states » corresponding to this periodic solution are used. During the trim process the inflow states are "refreshed" only after one rotor revolution, because they remain constant for one rotor revolution in order to represent a periodic solution (of the rotor states). Another *dynamic trim process* available for a time simulation solution process has been introduced in HOST for allowing strong coupling of time marching models (like CFD or the free wake model MINT) with the rotorcraft flight dynamics. The controls are dynamically adjusted as a function of time during the time simulation solution in order to satisfy the trim conditions.

In the RCAS trim solution, two methods are available for the periodic solution. Either an iterative solution for harmonic variables is obtained in the frequency domain (harmonic balance) or a time marching solution is obtained by integrating the equations in the time domain for successive time (azimuth) steps. In either case a periodic solution results. For either a specified periodic solution or a trim solution, the FSDI equations are expressed in terms of the DI states and these are solved together with the full vehicle equations of motion so that vehicle dynamic states and the DI states are obtained in the same solution process. For a trimmed periodic solution all of the states, including the DI states are periodically time varying. Consequently, the induced velocities that contribute to the blade angle of attack and the airloads are calculated from Eq. (1) using the periodically time varying DI states. The corresponding trim solution for the rotor controls yields the steady-state (constant) collective and cyclic pitch angles.

Description of the wind-tunnel test data

The wind-tunnel test data which serve as experimental reference for the present comparisons are those performed by NASA-Langley and the U.S. Army over a 10-year period beginning in the mid-1980s ([23] to [27]). Rotor inflow measurements were made with a laser velocimeter just above the blade (from one blade chord to half a chord) for a range of advance ratios from μ=0.15 to 0.40. The simplified helicopter model comprised a main rotor and a simple fuselage shape mounted independently beneath the rotor (Robin fuselage).

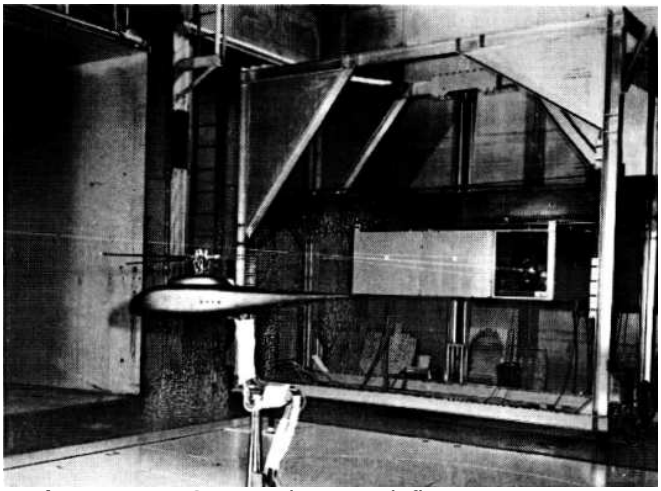

Figure 1 : NASA-Langley rotor inflow measurements with a laser velocimeter.

As discussed in [28], the effect of the fuselage on the rotor inflow is mainly an upwash tendency in the fore part of the rotor. On the rear part of the rotor, due to flow

detachment the fuselage effect can be neglected as sketched on **Figure 2**. In view of the slender shape of the Robin fuselage, the interference effect on the rotor airloads and flowfield is relatively small. In this paper all the calculations were done without taking into account the fuselage.

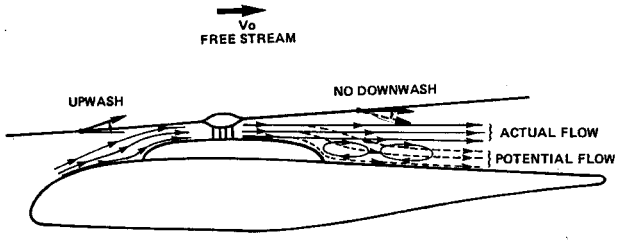

Figure 2 : Effect of fuselage on rotor inflow (extracted from [28]).

Two different sets of blades were used: rectangular and tapered blades. That turns out to be interesting since the effects of the blade planform on the induced flowfield can thus be assessed, especially at the tip of the blade.

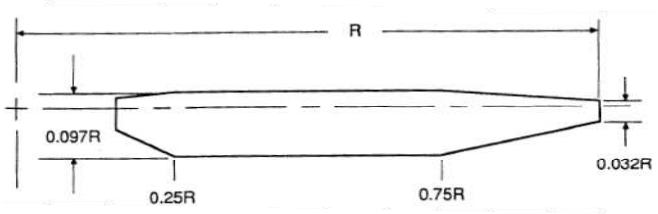

Figure 3 : Tapered blade plan-form.

The main characteristics of the two sets of blades are presented in [23]-[24]. Tab. 1 in appendix gives an overview of the test data for the two sets of blades and the different advance ratios. The case at μ=0.23 is the one for which the most measurements are available. At that advance ratio, measurements were made for the two sets of blades and at different heights above the TPP in the rectangular blade case. That is why most of the examples of comparisons shown on this paper concern that case. The effect of the height of measurements above the TPP (1 chord, 0.75 chord or 0.5 chord) can be seen on **Figure 4** and **Figure 5**.

The multiple measurements at different heights above the rotor disk provide a qualitative indication of the repeatability and reliability of the experimental data. (Note that the data in Figure 5 for the 0.75 and 0.5 chord measurement locations at r/R >0.6 of the advancing blade is considered to be incorrect). The induced velocities for the different measurement heights have generally similar radial distributions at the four azimuths, but closer to the rotor they are generally stronger. This general decrease in induced velocity with height above the rotor is consistent with the effect of wake induction. The significant effect of the measurement height will be important in comparisons of the experimental data with the FSDI calculated induced velocities since these calculations are restricted to the plane of the rotor disk.

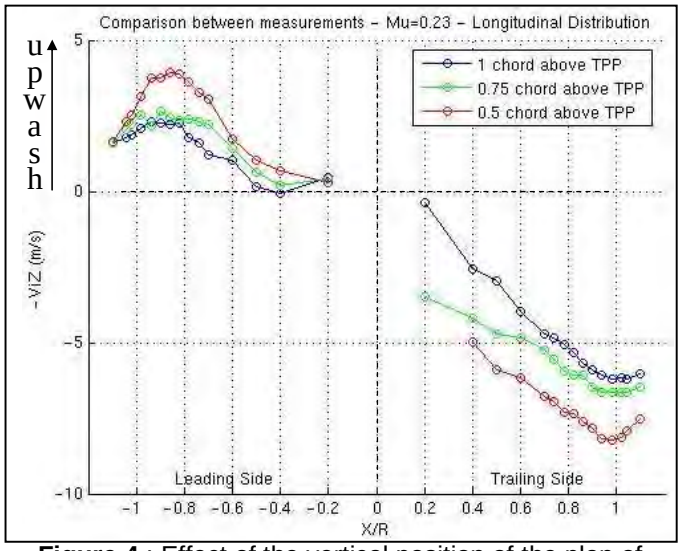

Figure 4 : Effect of the vertical position of the plan of measurement above the TPP on the longitudinal inflow distribution.

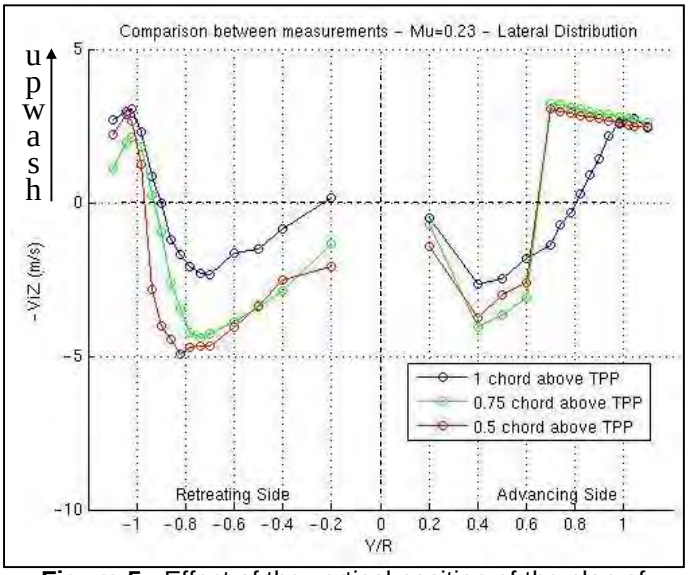

Figure 5 : Effect of the vertical position of the plan of measurement above the TPP on the lateral inflow distribution.

Before considering the calculations, it should be emphasized that the measurements herein were made in a plane above the rotor disk at fixed points in the non-rotating, disk-referenced, coordinate system. The measurements were performed instantaneously as a function of time and the data were also time averaged so that the results would be independent of the relative position of the blades with respect to the fixed points. Therefore two sets of data are available: the instantaneous and the time-averaged induced velocities; for the present paper, only the time-averaged velocities will be used to compare with the FSDI calculations. The measured data in **Figure 4** and **Figure 5** are the time-averaged induced velocities; in some later figures the time-averaged data will be accompanied by the max/min variations of the instantaneous induced velocity time histories at each measurement point.

Different kinds of calculations

In both codes (HOST & RCAS) as in any other rotorcraft simulation code using a lifting-line blade element model, the calculation of the aerodynamic forces requires the computation of the local relative air velocity including the contribution of the induced velocity at each blade element. These calculated local induced velocities at the blade element locations are the customary output results of the simulation codes and the ones that it would be of most interest to validate. However, these blade-referenced, on-blade, induced velocities cannot be directly measured experimentally and in fact exist only as a simple idealization for a lifting-line representation of a rotor blade. Nevertheless, the time (azimuth) varying on-blade velocities are often compared with rotor disk-referenced, time-averaged induced velocity measurements, and, in fact, most of the results presented in this paper will manifest this inconsistency. However, results will also be included that properly compare disk-referenced time-averaged FSDI calculations with the time-averaged experimental measurements and that will also show the error incurred by inconsistent comparisons.

For comparison and validation between simulation codes, it is logical and valid to compare the blade-referenced, on-blade induced velocity calculations as in this paper, although, due to the different trim processes used in the HOST and RCAS codes, most of the calculations were done using "average inflow states" for HOST and with "time varying inflow states" for RCAS. Again, the impact of these differences will be discussed below.

As a preliminary illustration of the sensitivity of the FSDI model to the order of truncation, several examples of rotor induced velocity fields calculated (on-blade) with "average inflow states" are presented on **Figure 6** with three different orders (or numbers of inflow states). These computations were done with FiSuW (FSDI model in HOST). They correspond to trim computations in the case at μ=0.23 with rectangular blades. The isolated rotor trim is performed by searching the three pitch rotor controls (collective and cyclic angles) that satisfy the three trim conditions: the rotor thrust (C_T=0.0064) and zero longitudinal and lateral flapping tilts of the rotor TPP. Once again, "average inflow states" means that the trim process provides at the end a constant set of inflow states representing the periodic solution found for the rotor steady state.

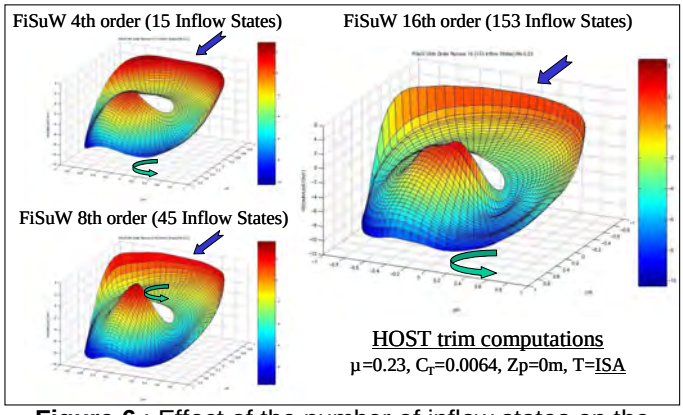

Figure 6 : Effect of the number of inflow states on the rotor induced velocity distribution, (rectangular blade case).

Calculations / test data comparisons

Comparisons of the HOST and RCAS induced velocity calculations with the experimental measurements will be presented for both the tapered and rectangular blade cases. The rectangular blade will involve additional consideration and discussion relative to the tapered blade case.

The **Figure 7** to **Figure 10** show examples of comparisons between HOST and RCAS as well as the test data at μ=0.15 for the tapered blade case. The calculations were done with the FSDI models at different orders (harmonics and radial polynomial order, h x f respectively) and with a vortex wake model (the free wake model MESIR in the HOST case). **Figure 7** concerns the longitudinal induced velocity distributions (azimuths 0° and 180°), **Figure 8** the lateral distributions (azimuths 90° and 270°) . **Figure 9** shows the azimuthal induced velocity distributions at r/R≈0.74 and **Figure 10** the azimuthal distributions at r/R≈0.90. HOST and RCAS comparisons are presented here side-by-side as the HOST induced velocities are in (m/s) and in RCAS in (ft/s). It should be noted that, as mentioned earlier, the HOST and RCAS results calculated using FSDI are the *blade-referenced* (time (azimuth) varying induced velocities in RCAS and time (azimuth) average induced velocities in HOST) while the test data are the *disk-referenced* time–averaged velocities as a function of disk azimuth. In addition, the HOST and RCAS results are calculated using a different trim process. Again, it is noted that the calculations are made for the rotor disk while the experimental measurements are obtained at 1 chord above the rotor disk.

All of the results are generally consistent and the HOST and RCAS computations are reasonably close for the same FSDI model orders. The effects of increasing the number of states are quite similar ("FiSuW 4th order" corresponds to "RCAS 4x4", "FiSuW 16th order" is roughly comparable to "RCAS 12x12"). Although there are differences between the HOST and RCAS vortex wake computations, as might be expected, the DI

calculations agree more closely with these vortex wake results when the number of states is increased. A difference between HOST/RCAS vortex calculations appears, RCAS calculations being smoother than in the HOST case. That could be due to different azimuthal resolution and/or vortex wake parameters (viscous core radius, etc.).

Compared to the test data, the calculations give the correct trends in terms of variations with the radius and azimuth. The downwash tendencies appear overestimated in the calculations, but as mentioned before, the measurements at one chord above the TPP underestimate the downwash (**Figure 4** and **Figure 5**). On the front part of the rotor (azimuths around 180°, see **Figure 9**), the calculations underestimate the upwash around r/R≈0.75 (see also **Figure 7** on the leading side). But that could be partly due to the effect of the fuselage (not included in the calculations).

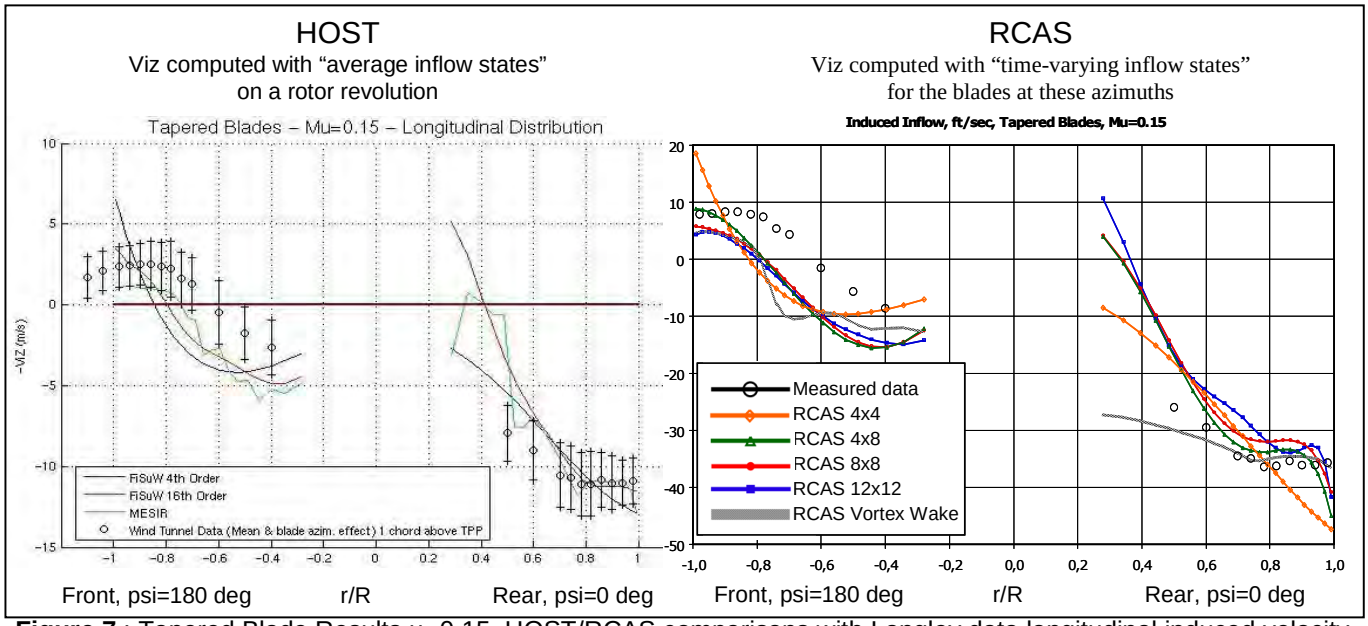

Figure 7 : Tapered Blade Results μ=0.15, HOST/RCAS comparisons with Langley data longitudinal induced velocity distribution.

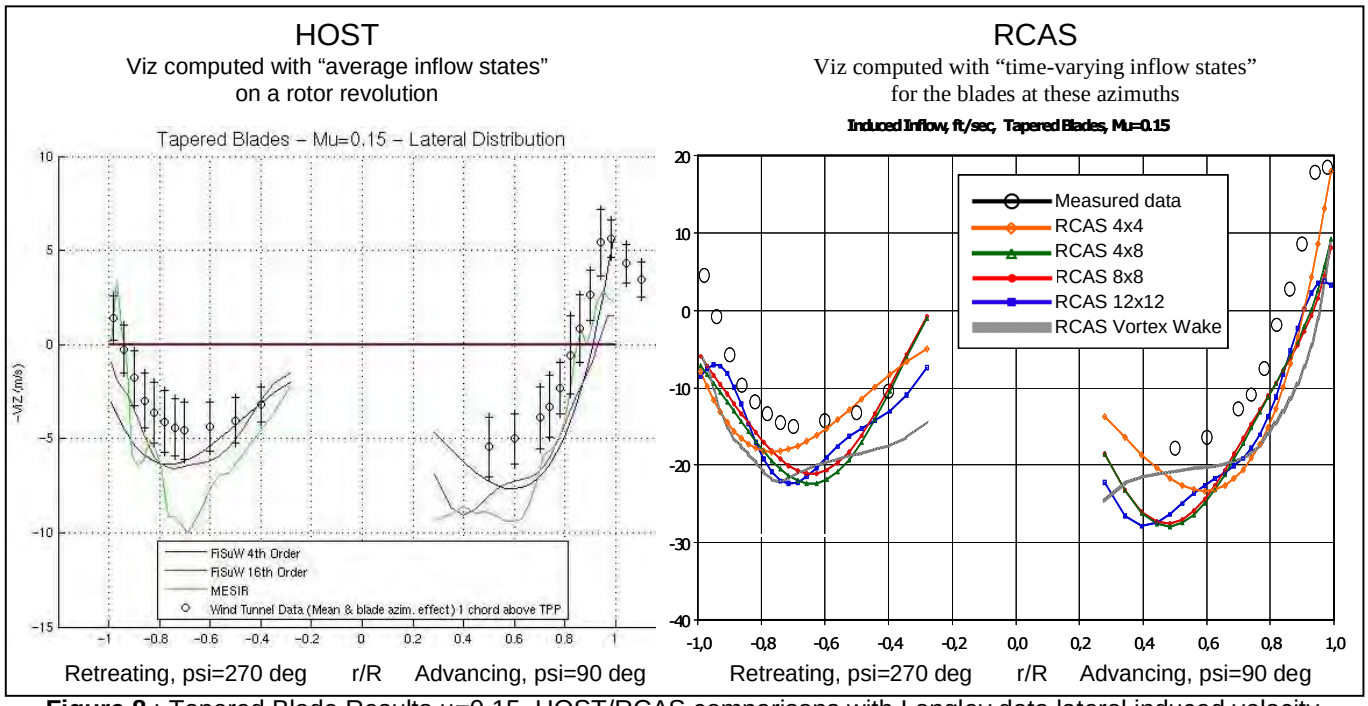

Figure 8 : Tapered Blade Results μ=0.15, HOST/RCAS comparisons with Langley data lateral induced velocity distribution.

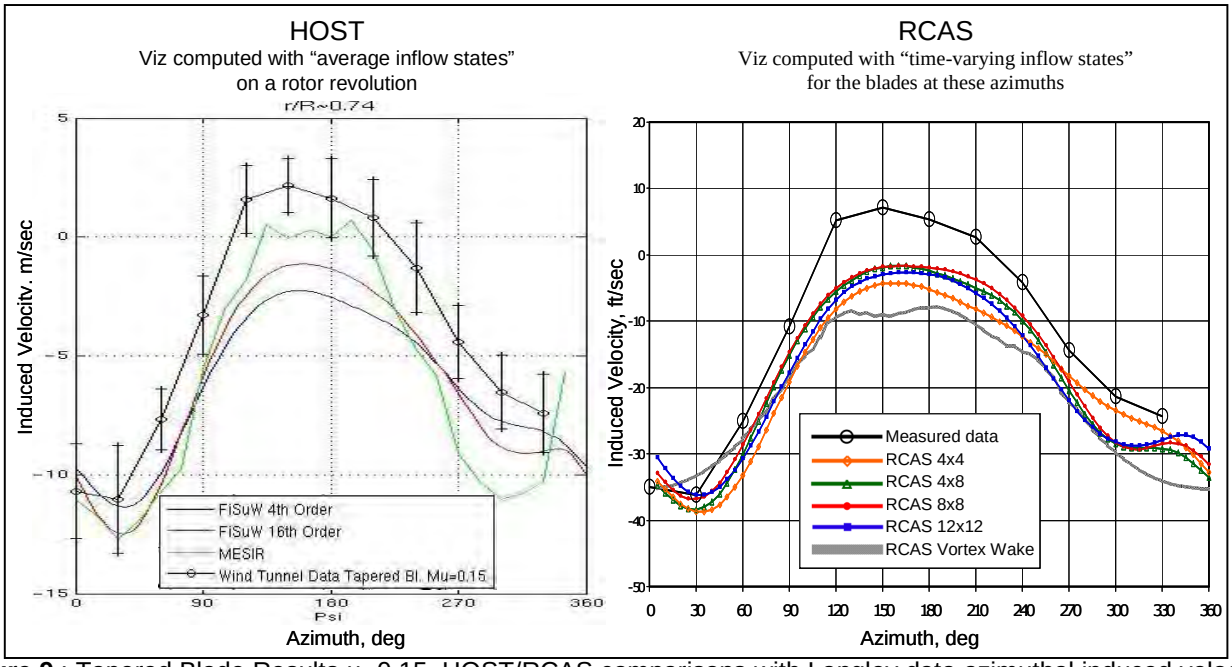

Figure 9 : Tapered Blade Results μ=0.15, HOST/RCAS comparisons with Langley data azimuthal induced velocity distribution at r/R~0.74.

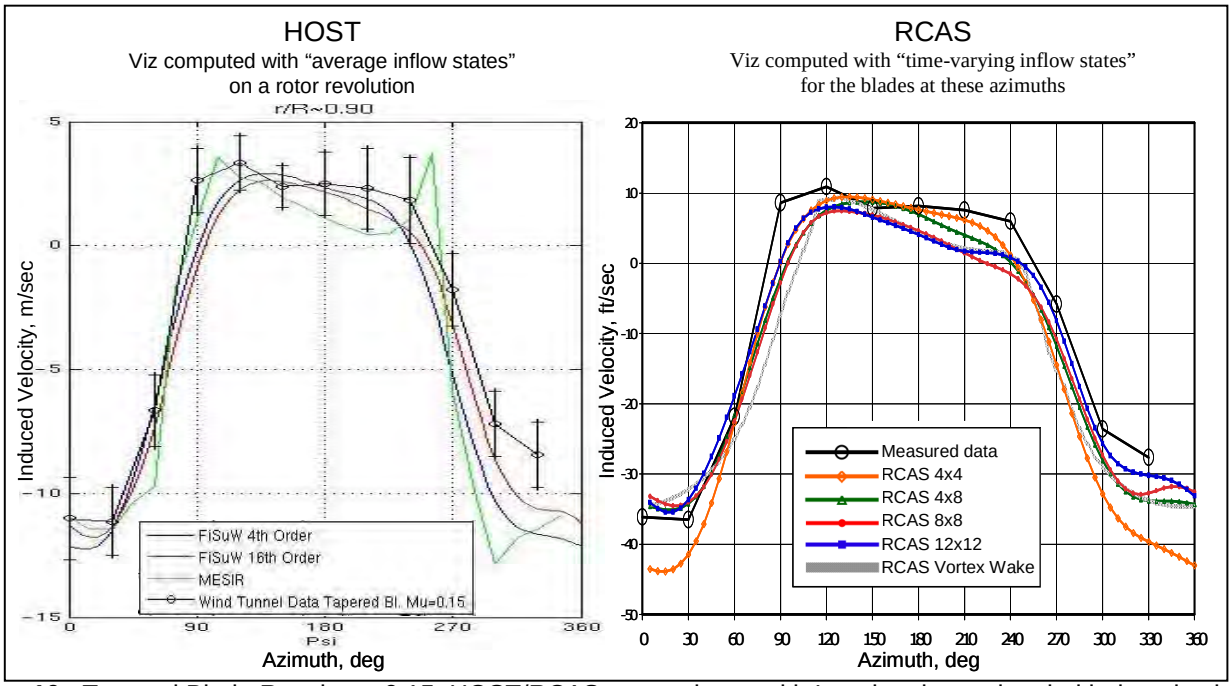

Figure 10 : Tapered Blade Results μ=0.15, HOST/RCAS comparisons with Langley data azimuthal induced velocity distribution at r/R~0.9.

The next results address the effect of using FSDI calculations for disk-referenced time-averaged induced velocities to compare with the experimental measurements rather than the blade-referenced (on-blade) calculations. The time-averaged velocity calculations are more appropriate for these comparisons with the time-averaged experimental measurements. Here the FSDI time-averaged calculations were made with the FLIGHTLAB simulation code (Advanced Rotorcraft Technology, Inc.) rather than with RCAS but the implementation of the FSDI theory is similar to the method used in RCAS.

Figure 11 and **Figure 12** show for the same case (μ=0.15, tapered blades) an example of comparison of the FLIGHTLAB results with the experimental data and the RCAS calculations for the same order of truncation (4th order in harmonics and 8th order in radial mode

shape functions, h x f = 4 x 8). The comparisons between RCAS and FLIGHTLAB "time-varying" results are nearly identical as they should be (in the figure legend, "time-varying" refers to the on-blade time-varying velocities presented earlier). The FLIGHTLAB disk-referenced, time-averaged calculations are now compared consistently with the time-averaged measured test data and they compare better than the blade-referenced "time-varying" velocities. The effect is mainly significant near the tip of the blade where the downwash of the tip vortex amplifies the induced (downwash) velocity in the case of the blade-referenced calculation (since it moves with the blade) relative to the time-averaged result where the tip vortex only contributes when the blade passes the azimuth of the disk-referenced measurement point.

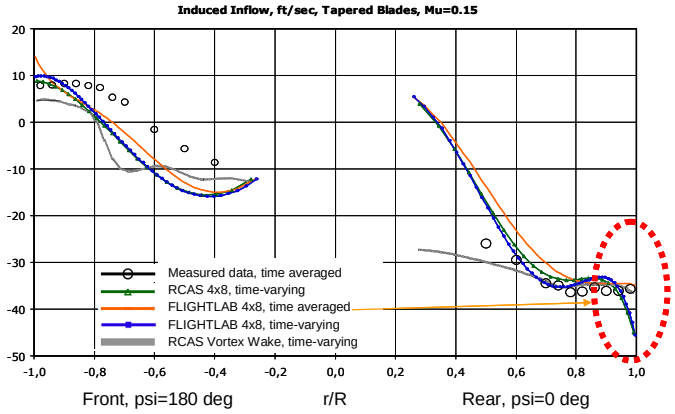

Figure 11 : Effect of average vs time-varying calculations, RCAS/Flightlab comparisons with Langley data longitudinal induced velocity distribution.

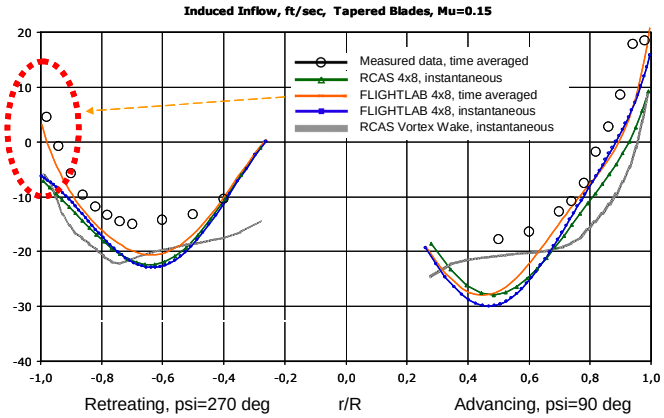

Figure 12 : Effect of average vs time-varying calculations, RCAS/Flightlab comparisons with Langley data lateral induced velocity distribution.

Compared to harmonic trim results obtained with HOST, it should be emphasized that using "average inflow states" for calculating blade-referenced induced velocities is in principle not equivalent to time-averaged disk-referenced induced velocities. It could be thought that it is the same by considering the local induced velocity development (see Eq. 1), where the time and space dependencies are separated with the inflow states being the only terms depending on the time. Theoretically and rigorously that is not identical, but in practice the HOST results are close to the FLIGHTLAB "time average" results (see **Figure 11** and **Figure 7**).

The following figures (**Figure 13** to **Figure 18**) show the comparisons in the rectangular blade case. The effect of the different HOST and RCAS trim processes is more sensitive for the rectangular blade case. The difference appears mainly near the blade tip and is especially striking on the front part of the rotor (**Figure 13**). This effect is magnified when increasing the number of inflow states, see **Figure 15** and **Figure 16** which show the effects of using truncations at the 4th and 8th orders respectively for the case at μ=0.30.

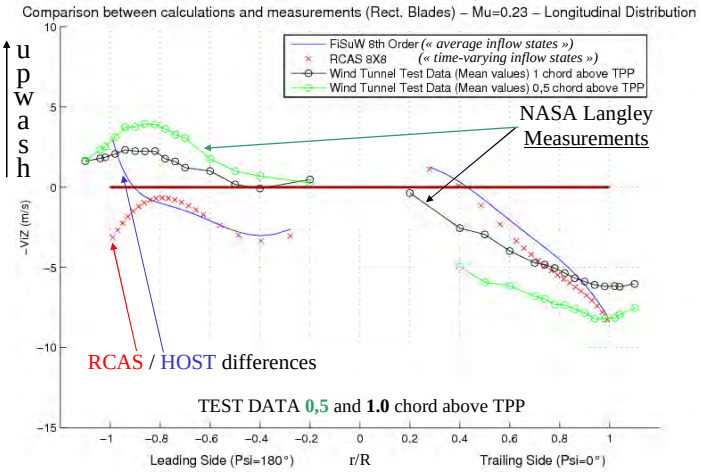

Figure 13 : Rectangular blade results μ=0.23, HOST/RCAS comparisons (45 IS) with Langley data longitudinal induced velocity distribution.

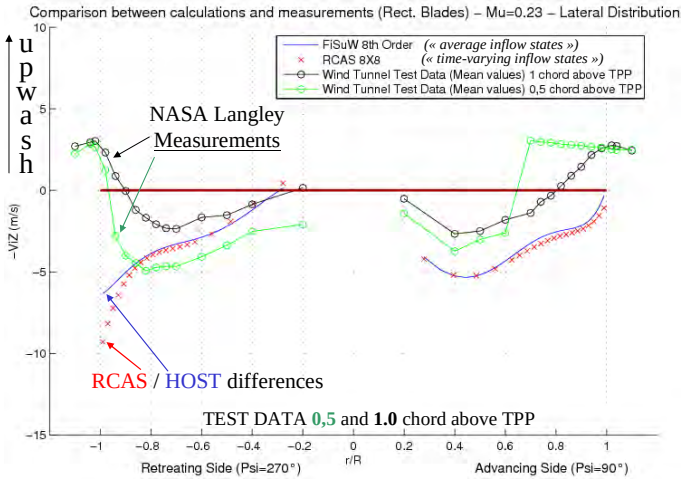

Figure 14 : Rectangular blade results μ=0.23, HOST/RCAS comparisons (45 IS) with Langley data lateral induced velocity distribution.

Compared to the test data, the general tendencies of the induced velocity distributions are reasonably well predicted by the FSDI model. Yet as for the tapered blade case, the calculated downwash looks overestimated for the lateral distribution (when compared with measurements at one chord above TPP which underestimates the downwash) and the upwash on the front of the rotor is underestimated by the calculations. The agreement with rectangular blade test data is however not so good as for the tapered blade case. A similar difference between comparisons of FSDI calculations with the tapered and rectangular blade measurements has been reported in the literature (e.g. [29]). A significant discrepancy with test data appearing in the rectangular blade case can be seen near the tip of the retreating blade (left part of the lateral distributions on **Figure 14**, **Figure 15** and **Figure 16**).

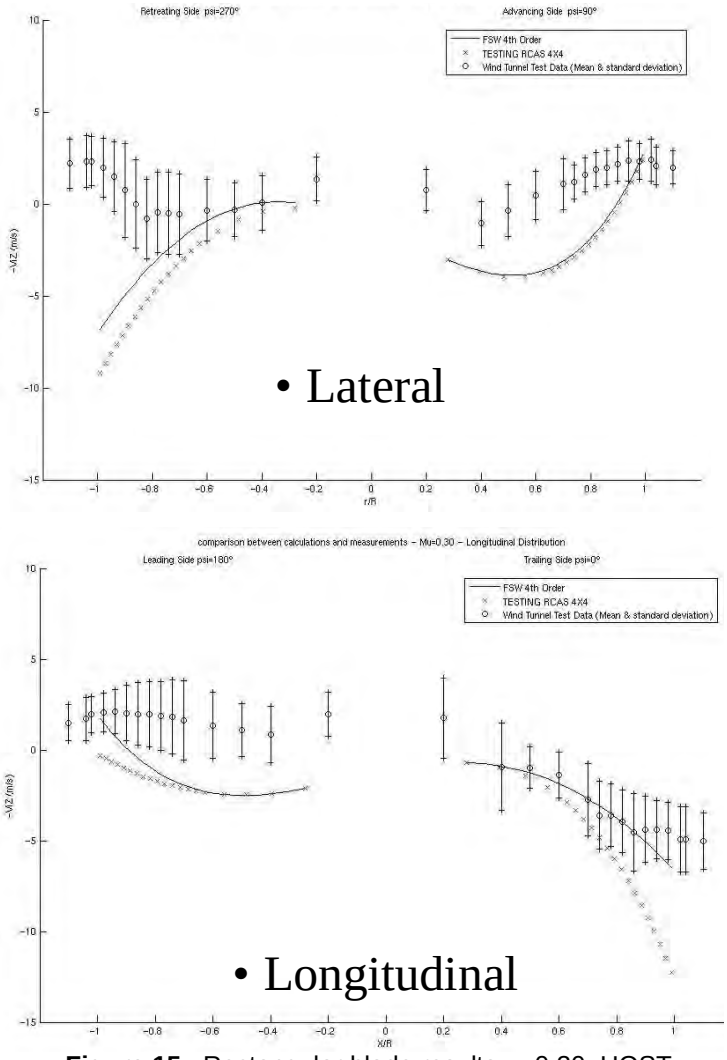

Figure 15 : Rectangular blade results μ=0.30, HOST (blue) / RCAS (red) comparisons (4th order, 15 IS) with Langley data induced velocity distribution 1chord above.

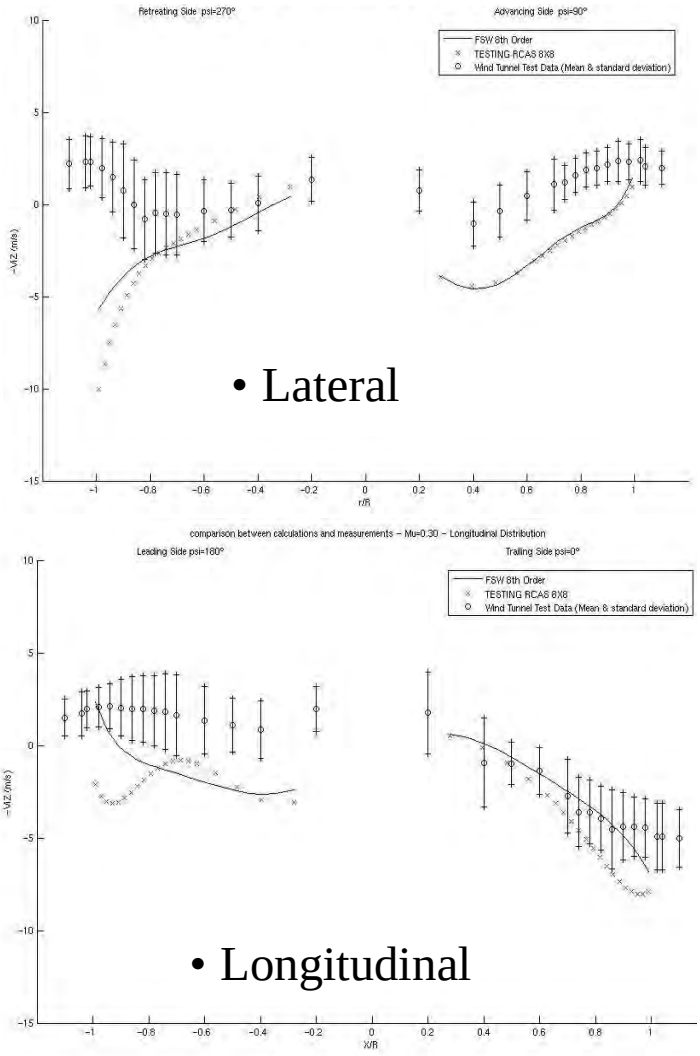

Figure 16 : Rectangular blade results μ=0.30, HOST (blue) / RCAS (red) comparisons (8th order, 45 IS) with Langley data induced velocity distribution 1chord above.

The RCAS results that use the trim procedure with periodically time varying inflow states (RCAS results are red cross symbols in the figures) increase the downwash near the tip of the retreating blade and also in a lesser amount on the rear blade position when using a 4th order model (15-states). However, this is partly the effect of using the blade-referenced time-varying calculation results rather than the time-averaged results as shown with the HOST calculations for the retreating blade. This inconsistency is expected to be magnified in the case of the rectangular blades.

The overestimation of the downwash near the tip of the retreating blades both with HOST and RCAS is the most striking disagreement with the rectangular blade test data. The fact that this is not evident in the comparisons with tapered blade measurements (see **Figure 8**) suggests a possible a weakness in the FSDI theory.

In the calculations for the tapered blade case, the lift is significantly reduced near the blade tip due to the reduced chord of the tapered planform. In contrast, the lift distribution of the rectangular blade increases continuously with radius out to the blade tip. Experience with the convergence characteristics of the FSDI theory indicates that achieving accurate blade airloads and corresponding induced velocity distributions is dependent on using a high order model involving a large number of states. This is increasingly true in the blade tip region. And since the rectangular blade increases the blade tip lift distribution relative to the tapered blade, it is not surprising that the discrepancies in comparisons with experimental data may be larger for rectangular blades. With respect to convergence, it turns out that even with a model truncated at the 16th order (153 IS) the rectangular blade results are not fully satisfactory. A very high order model would raise problems of computational time.

For practical applications, this problem may be treated by introducing an empirical blade lift tip loss especially for non-tapered blades. It must be recognized that this approach is inconsistent with the rigorous fluid mechanics foundation of the FSDI theory. Simple approximations to rotor inflow (e.g., momentum theory) cannot model wake induction effects to satisfy the zero lift boundary condition at the tip of a wing or rotor blade and must resort to an ad hoc tip loss factor. Properly formulated vortex wake models as well as the FSDI theory inherently model the mutual interaction of the wake induced velocity and the blade lift distribution to satisfy the blade tip boundary condition.

In the FiSuW model in HOST, an empirical means of improving the satisfaction of the boundary condition is discussed here. A limit condition imposing zero lift at the blade tip section has been introduced with a test for checking if the blade tip section represents a small enough part of the blade span (lesser or equal to 3%). Plots generated by FLIGHTLAB using the 4 x 6 DI model (24 states) with a tip loss correction have been provided by Advanced Rotorcraft Technology, Inc. for the rectangular blade case at μ=0.15. The comparisons are quite good in **Figure 17** between the red curves produced by FiSuW with the blade tip loss limit condition ("+Lift(R)=0") and the FLIGHTLAB results (both time-averaged and time-varying blade-referenced FLIGHTLAB calculations are included and they are similar in this case). Both HOST and FLIGHTLAB predict a decrease of the downwash near the tip of retreating blade which is in better agreement with the general trends of the test data even though for the case μ=0.15 the experimental data are unfortunately not available for that azimuth (270°).

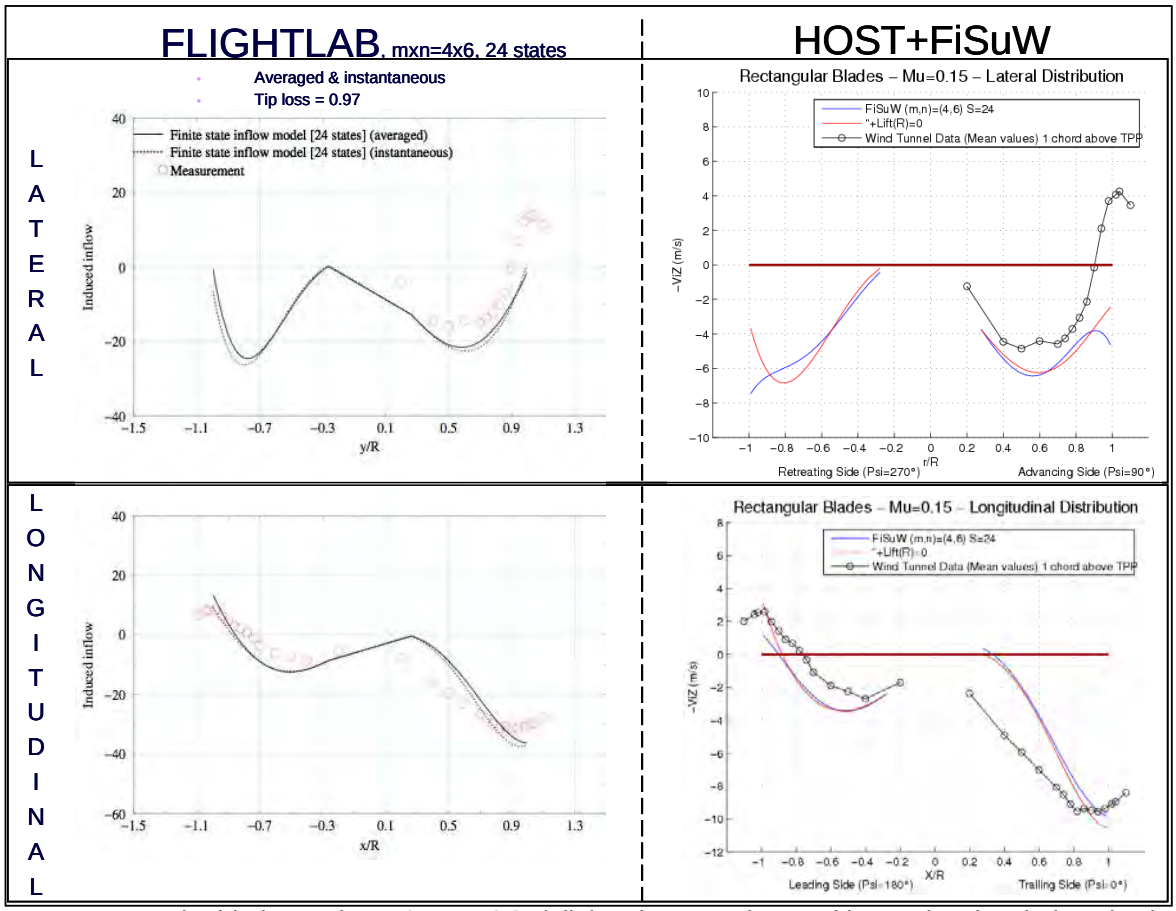

Figure 17 : Rectangular blade results μ=0.15, HOST/FlightLab comparisons with Langley data induced velocity distributions (effect of the blade lift tip loss).

The comparisons of "HOST+FiSuW" with the test data can also be seen in **Figure 18** presenting the lateral induced velocity distributions for the rectangular blade case at μ=0.23. With the lift tip loss condition (red curves), the discrepancy with the test data due to the downwash predicted at the tip of the retreating blade is clearly reduced. Now the FiSuW calculations indicate an upwash at the tip improving also the correlation with experimental data at the tip of the advancing blade.

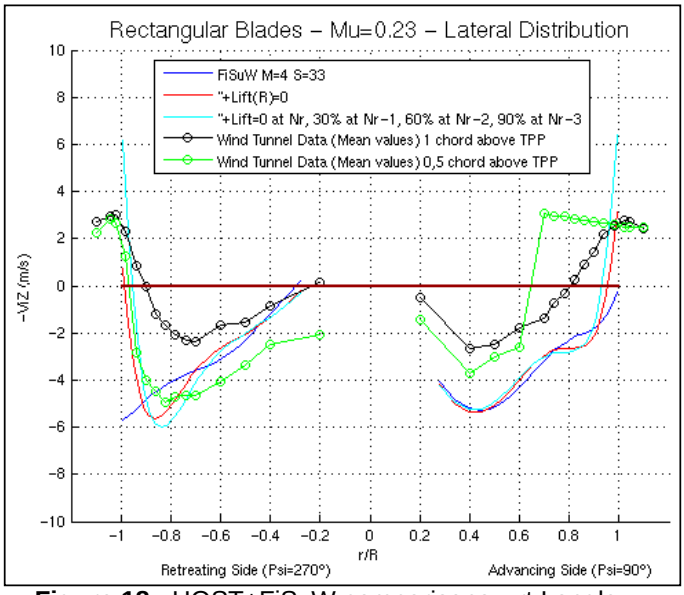

Figure 18 : HOST+FiSuW comparisons wrt Langley lateral rotor inflow measurements above rectangular blades at μ=0.23 (effect of the blade lift tip loss).

As noted above, applying a tip-loss correction to the FSDI theory is not rigorous, but in some respects empirically compensates for poor convergence of low-order models. Reflection on the physical behavior of the tip loss model may lend some insight as to the reasons for the improvements. Physically, applying a tip-loss correction to FSDI theory is equivalent to reducing the effective lifting radius of the rotor. Since the region just beyond the tip of a wing or rotor blade reflects the upwash of the tip vortex, the tip loss correction moves this upwash region radially inward. This is evident in **Figure 18** for both the advancing and retreating blade tips. In fact the larger of the two tip loss corrections seems to exaggerate this effect (when compared with the one chord above TTP measurement, but not with the 0.5 chord case), and while it tends to improve the comparison with the measured induced velocity near the tip, it tends to degrade the shape of the radial distribution of induced velocity (when compared with 1 chord height case). Again, it must be noted that the effects of measurement height above the rotor disk are large and the calculations are only valid at the rotor disk.

In view of the various differences and inconsistencies between the present calculated results and the Langley experimental data, a few final comments are in order. Rotor flowfield calculations based on more sophisticated computational methods have been compared with the Langley data (published in recent years [31]-[32]) that are highly relevant with regard to the present investigation. These recent results address all of the limitations of the present investigation. For example, both time-averaged and time-varying disk-referenced induced velocities are calculated for comparison with the experimental data. The calculations also include the Robin fuselage and are performed for the same heights above the rotor disk used for the experimental measurements. In addition to the normal component of the induced velocity, the calculated streamwise component is also compared with the measurements. Finally, a variety of results are presented for various advance ratios and azimuth angles, including the more challenging rectangular blade. In general, the correlations presented in these studies are excellent. This tends to increase confidence in the Langley experimental data and confirm that deficiencies in the present correlations are the result of inconsistencies in the comparisons or limitations of the FSDI theory. Of course the success of the calculations in [31]-[32] comes at a cost of versatility and computational burden. Given the objectives and intended purpose of the FSDI theory previously reported, the present comparisons with experimental data are remarkably good.

Comparisons between DI calculations on a simplified academic case

One objective of the US-France MOA task on which the present results are based was to verify the independent implementations of the FSDI in the HOST and RCAS codes. When differences between the HOST and RCAS calculated results were found during comparisons with the Langley rotor model induced velocity measurements, a simplified rotor problem was defined to help diagnose the source of the differences. As discussed earlier, several differences in the two implementations were found, the most significant being the difference in the trim calculation process where the HOST code uses the time (azimuthal) averaged DI states to calculate the induced velocities. In order to better compare the calculations of HOST and RCAS FSDI models directly, and mutually validate the two implementations, the simplified rotor problem, different from the wind-tunnel rotor test was used. This is called the simplified academic case since it avoids modifying the HOST and RCAS codes to make a direct comparison for a typical rotor problem such as the wind tunnel cases.

For this simplified academic case, the rotor and blade characteristics of the rectangular blade set are still used as input data, except that here a simple linear airfoil model was adopted ($C_l=2\pi\times(\alpha-\alpha_0)$ with α_0 =-8.6deg ; $C_d=C_m=0$).

In order to avoid the differences in the airload coordinate systems used in the HOST and RCAS implementations, the blade flap and lead-lag hinges are removed and the

blade collective and cyclic pitch angles are specified to be zero. Thus the orientation of the blade and rotor TPP coordinate systems as employed in the HOST and RCAS FSDI implementations are identical. Although the rotor collective pitch angle is set to zero, rotor thrust, and hence induced flow, is produced by the -8.6 deg zero lift angle of the blade airfoil. Since the pitch controls are specified in advance, the iterative trim calculations in HOST and RCAS are not required, only a periodic solution for the aerodynamic and FSDI equations of motion is needed. Notice that since the pitch angles are imposed, this is not a trim case but a calculation for fixed arbitrary identical conditions: 400km/h, sea-level, ISA (Zp=0m, T=15℃), and the rotor mast is vertical.

Very good agreement was obtained between HOST FiSuW model and RCAS DI model for the time-averaged inflow states, but not for the blade-referenced (on-blade) induced velocities as shown in **Figure 19**; compare the HOST results in red with RCAS results in blue. To investigate the reasons for the difference, the RCAS calculations for the academic test case were next performed by imposing the HOST rotor blade lift airload distributions in place of the RCAS airloads as shown by the results labelled "RCAS_HOST" in green in **Figure 19**. But the discrepancy in the induced velocity distributions still remained. That is in fact due to different methods used in HOST and RCAS to calculate the blade-referenced (on-blade) induced velocities from the inflow states.

In HOST even though the academic test case did not involve an actual trim, the computation of the induced velocity was made by using the same process, i.e. the induced velocities are calculated with "time-averaged inflow states" based on one rotor revolution. In RCAS the blue and green results were calculated with time- (or azimuth-) varying inflow states ($\psi_{blade}= \Omega t$). In order to duplicate the HOST process, the "average inflow states" were then also used to calculate the induced velocities in RCAS and the results (grey squares) coincided perfectly with the induced velocities calculated directly with HOST (red curves) on **Figure 19**, thus identifying the source of the difference between the two codes. This agreement between the two codes is proof of mutual validation.

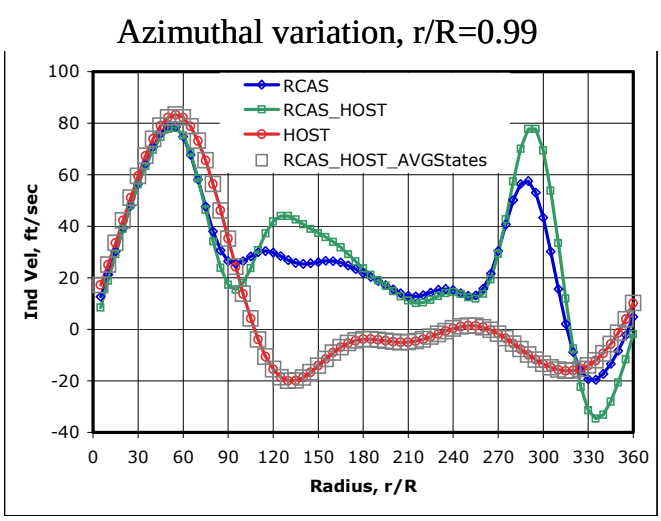

Figure 19 : HOST/RCAS induced velocity fields comparisons on an academic case, azimuthal distributions at r/R=0.99.

Conclusions

With regard to the comparisons between the HOST FiSuW model and the RCAS FSDI model:

- theoretically, they are both based on the same dynamic inflow theory as presented in [1] and [2] (except on the mean inflow parameter, but HOST includes the two expressions for that term);
- practically, or numerically, the two implementations manifest the following main differences:
  - differences in coordinate frame both for the lift distribution inputs and for the induced velocity outputs: the implementation in HOST is presently made in the blade coordinate system, whereas RCAS uses the rotor disk (TPP) coordinate system;
  - differences in the trim process: for steady state (trim and periodic solutions) computations (in contrast to transient time simulations), HOST searches for periodic solution for rotor states meaning a constant set of inflow states called here "average inflow states" based on one rotor revolution, while RCAS uses the full "time (or azimuthwise) varying inflow states" when solving for a periodic time solution;
  - in HOST a lift tip loss condition has been introduced (enabling in practice to mitigate the poor convergence characteristics of the FSDI theory near the blade tip).

About the comparisons with the test data and vortex wake model calculations:

The calculations with FSDI models are generally in good agreement with the test data contributing to the validation of these models. The comparisons are better in the tapered blade case than in the rectangular blade case. For the rectangular blade case the introduction of a blade

lift tip loss limit condition helps in practice the FSDI models to converge toward a more realistic inflow distribution near the blade tip.

Increasing the number of inflow states refines the level of detail of the induced velocity distributions. The higher the number of inflow states (or order of truncation), the closer the FSDI model induced velocity distributions agree with the ones calculated with vortex wake models.

This paper draws the attention on the importance of comparing the same kind of induced velocity distributions either between calculations or between calculation and test data. In particular, the blade-referenced (on-blade) time-varying induced velocity and the disk-referenced time-averaged velocities are distinguished. Calculations of the latter are appropriate for comparisons with the time-averaged experimental data and were, in fact, in better agreement in the case of the few FLIGHTLAB results presented. It is also noted that the calculations made on the rotor disk were compared to measurements made above the disk and this inconsistency accounted for some important differences observed in the comparisons.

Acknowledgements

Both authors thank Drs. Hossein Saberi and Chengjian He of Advanced Rotorcraft Technology, Inc. for their kind and useful contributions. The French author would like to thank the ONERA Scientific Direction for the funding in this study.

References

[1] Peters D.A. and He C.J., "A Closed-Form Aerodynamic Theory for Lifting Rotors in Hover and Forward Flight", American Helicopter Society 43rd Annual Forum, Saint Louis, Missouri, May 18 - 20, 1987.

[2] He C.J., "Development and Application of a Generalized Dynamic Wake Theory for Lifting Rotors", Ph.D. Dissertation, Georgia Institute of Technology, August, 1989.

[3] D.A. Peters, C. He, “Finite State Induced Flow Models. Part II : three-dimensional rotor disk”, Jal of the Aircraft, vol. 32, n°2, March-April 1995.

[4] Peters D.A., Hsieh M.C., Garcia-Duffy C., “A complete finite-state inflow theory from the potential flow equations”, 3rd International Basic Research Conference on Rotorcraft technology, Nanjing, China, Oct. 14-16, 2009.

[5] P. Rebuffet, “Experimental aerodynamics- Chap. 73 Froude Theory”, Ed. Dunod, Paris, 1969.

[6] H. Glauert, “A general theory of the autogyro”, Reports and Memoranda n°1111, British A.R.C., 1926.

[7] J. Meijer-Drees, “A theory of airflow through rotors and its application to some helicopter problems”, Jal of the Helicopter Association of Great Britain, Vol. 3, n° 2, July-Sept. 1949.

[8] R.P. Coleman, A. M. Feingold, C. W. Stempin, “Evaluation of the induced velocity field of an idealized helicopter rotor”, NACA ARR L5E10, Washington, June 1945.

[9] F. White, B. B. Blake, “Improved Method of Predicting Helicopter Control Response and Gust Sensitivity”, A.H.S. Annual Forum, May 1979.

[10] D.M. Pitt, D.A. Peters, "Theoretical prediction of dynamic inflow derivatives", Vertica, vol. 5, pp. 21-34, 1981.

[11] D.M. Pitt, D.A. Peters, "Rotor dynamic inflow derivatives and time constants from various inflow models", 19th European Rotorcraft Forum, Stresa (Italy), September 1983.

[12] D.A. Peters, N. Haquang :“Dynamic inflow for practical applications”, Jal of the American Helicopter Society, T. N., vol. 33, n°4, pp. 64-68, October 1988.

[13] J. Delville, “The Proper Orthogonal Decomposition and the analysis of the 3D-structure of the free sheared turbulent flows”, Doctoral Thesis Dissertation, University of Poitiers, 1995.

[14] W. Kinner, “Die Kreisformige Tragfläche auf Potentialtheorischer Grundlage”, Ingenieur Archiv, vol. 7, 1937/ “Theory of Circular Wing”, Translation n° 234 5, Ministry of Aircraft Production, UK.

[15] P.-M. Basset, "Modeling of the dynamic inflow on the main rotor and the tail components in helicopter flight mechanics", 22nd European Rotorcraft Forum, Brighton (UK), paper n°104, September 1996.

[16] P.-M. Basset, F. Tchen-Fo, "Study of the rotor wake distortion effects on the helicopter pitch-roll cross-couplings", 24th European Rotorcraft Forum, Marseilles (France), paper n°FM06, September 1998.

[17] P.-M. Basset, A. El Omari, "A rotor vortex wake model for helicopter flight mechanics and its application to the prediction of the pitch-up phenomenon", 25th E.R.F., Rome (Italy), paper n°H08, September 1999.

[18] M. Hamers, P.-M. Basset, “Application of the Finite State Unsteady Wake Model in Helicopter Flight Dynamic Simulation”, 26th European Rotorcraft Forum, September 2000.

[19] B. Benoit, A.-M. Dequin, P.-M. Basset, B. Gimonet, W. von Grünhagen, K. Kampa, "HOST, a general helicopter simulation tool for Germany and France", 56th Annual Forum of the American Helicopter Society, Virginia Beach (US), Mai 2000.

[20] Basset P.-M. et al., “Finite state rotor induced flow model for interference and ground effect”, 57th Annual Forum of the American Helicopter Society, Mai 2001.

[21] Ormiston R.A., “A New Formulation for Lifting Rotor Performance Including Comparison with Full-Scale Data”, AHS International 64th Annual Forum and Technology Display, Montreal, Quebec, Canada, April 29 - May 1, 2008.

[22] Gorton S.A, Hoad D.R. : “Assessment of Rotor Blade Angle of Attack from Experimental Inflow Data”, Journal of Aircraft, Vol. 39, N°5, September-October 2002.

[23] Elliott J. W., Althoff S. L.:
NASA Technical Memorandum 100541 to 100543, April 1988.
“Inflow measurement made with a laser velocimeter on a helicopter model in forward flight”,
NASA-TM 100541, Volume 1, “Rectangular planform blades at an advance ratio of 0.15”,
NASA-TM 100542, Volume 2, “Rectangular planform blades at an advance ratio of 0.23”,
NASA-TM 100543, Volume 3, “Rectangular planform blades at an advance ratio of 0.30”.

[24] Althoff S. L., Elliott J. W.:
NASA Technical Memorandum 100544 to 100545, April 1988.

"Inflow measurement made with a laser velocimeter on a helicopter model in forward flight",
NASA-TM 100544, Volume 4, "Tapered planform blades at an advance ratio of 0.15",
NASA-TM 100545, Volume 5, "Tapered planform blades at an advance ratio of 0.23".

[25] Hoad D. R., Althoff S. L., Elliott J. W.:
NASA Technical Memorandum 101598 to 101599, April 1989.
"Inflow measurement made with a laser velocimeter on a helicopter model in forward flight",
NASA-TM 101598, Volume 6, "Rectangular planform blades at an advance ratio of 0.35",
NASA-TM 101599, Volume 7, "Rectangular planform blades at an advance ratio of 0.40".

[26] Althoff S. L., Elliott J. W., Hoad D. R.:
NASA Technical Memorandum 102642 to 102645, May 1990.
"Inflow measurement made with a laser velocimeter on a helicopter model in forward flight",
NASA-TM 102642, Volume 8, "Rectangular planform blades at an advance ratio of 0.23, 0.50 chord above the Tip Path Plane",
NASA-TM 102643, Volume 9, "Rectangular planform blades at an advance ratio of 0.23, 0.75 chord above the Tip Path Plane",
NASA-TM 102644, Volume 10, "Rectangular planform blades at an advance ratio of 0.30, 0.50 chord above the Tip Path Plane",
NASA-TM 102645, Volume 11, "Rectangular planform blades at an advance ratio of 0.30, 0.75 chord above the Tip Path Plane".

[27] Hoad D. R., Althoff S. L., Elliott J. W.: "Rotor inflow variability with advance ratio", 44th Annual Forum of the American Helicopter Society, Washington, D.C., June 1988.

[28] Dehondt A., Toulmay F.: "Influence of fuselage on rotor inflow performance and trim", Vertica, Vol. 14, N°4, pp 573-585, 1990.

[29] Peters D. A., He C. J.: "Correlation of measured induced velocities with a finite-state wake model", 45th Annual Forum of the American Helicopter Society, Boston, Mass., May 1989.

[30] Boyd D. .D., Barnwell R. W., Gorton S. A.: "A computational Model for Rotor-Fuselage Interactional Aerodynamics", AIAA 200-0256, 38th Aerospace Sciences Meeting & Exhibit, reno, NV, January 10-13 2000.

[31] Park Y. M., Nam H. J., Kwon O. J.: "Simulation of Unsteady Rotor-Fuselage Interactions Using Unstructured Adaptive Meshes", 59th Annual Forum of the American Helicopter Society, Phoenix, Arizona, May 6-8 2003.

[32] Kenyon A. R., Brown R. E.: "Wake Dynamics and Rotor - Fuselage Aerodynamic Interactions", 63rd Annual Forum of the American Helicopter Society, Virginia Beach, VA., May 1-3 2007.

	ADVANCE RATIO μ VH = μ * VTIP (km/h)		**0,15 103,043**	**0,23 157,998**	**0,30 206,085**	**0,35 240,433**	**0,40 274,78**
	AlphaShaft		**-3 deg**	**-3.04 deg**	**-4.04 deg**	**-5.70 deg**	**-6.80 deg**
BLADES	**Rectangular Planform**	Distance of measure above tip path plane	1 chord (Vol.1)	1 chord (Vol.2)	1 chord (Vol.3)	1 chord (Vol.6)	1 chord (Vol.7)
				0,5 chord (Vol.8)	0,5 chord (Vol.10)		
				0,75 chord (Vol.9)	0,75 chord (Vol.11)		
	Tapered Planform		1 chord (Vol.4)	1 chord (Vol.5)			

Tab. 1 : synoptic table of the NASA-Langley rotor inflow measurements used here ([23][24][25][26]).